Published in final edited form as:
Bioorg Med Chem. 2011 June 1; 19(11): 3347–3356. doi:10.1016/j.bmc.2011.04.042.

SAR Studies of 4-Pyridyl Heterocyclic Anilines that Selectively Induce Autophagic Cell Death in von Hippel-Lindau-Deficient Renal Cell Carcinoma Cells

Muriel Bonnet[a], **Jack, U. Flanagan**[a], **Denise A. Chan**[b,1], **Edwin W. Lai**[b], **Phuong Nguyen**[b], **Amato J. Giaccia**[b], and **Michael P. Hay**[a,*]

[a]Auckland Cancer Society Research Centre, The University of Auckland, Auckland, New Zealand
[b]Department of Radiation Oncology, Stanford University School of Medicine, Stanford, CA 94305, USA

Abstract

We recently identified a class of pyridyl aniline thiazoles (PAT) that displayed selective cytotoxicity for von Hippel-Lindau (VHL) deficient renal cell carcinoma (RCC) cells in vitro and in vivo. Structure-activity relationship (SAR) studies were used to develop a Comparative Molecular Field Analysis (CoMFA) model that related VHL-selective potency to the three dimensional arrangement of chemical features of the chemotype. We now report the further molecular alignment-guided exploration of the chemotype to discover potent and selective PAT analogues. The contribution of the central thiazole ring was explored using a series of 5- and 6-membered ring heterocyclic replacements to vary the electronic and steric interactions in the central unit. We also explored a positive steric CoMFA contour adjacent to the pyridyl ring using Pd-catalyzed cross-coupling Suzuki-Miyaura, Sonogashira and nucleophilic displacement reactions to prepare of a series of aryl-, alkynyl-, alkoxy- and alkylamino-substituted pyridines, respectively. In vitro potency and selectivity were determined using paired RCC cell lines: the VHL-null cell line RCC4 and the VHL-positive cell line RCC4-VHL. Active analogues selectively induced autophagy in RCC4 cells. We have used the new SAR data to further develop the CoMFA model, and compared this to a 2D-QSAR method. Our progress towards realizing the therapeutic potential of this chemotype as a targeted cytotoxic therapy for the treatment of RCC by exploiting the absence of the VHL tumor suppressor gene is reported.

Keywords

drug design; structure-activity relationships; renal cell carcinoma; autophagy; von Hippel Lindau; Suzuki-Miyaura; Sonogashira; QSAR

*Corresponding author, Address: Auckland Cancer Society Research Centre, The University of Auckland, Private Bag 92019, Auckland 1142, New Zealand. Tel: +649 923 6598; fax: +649 373 7502. m.hay@auckland.ac.nz.
[1]Present address: Department of Radiation Oncology, University of California, San Francisco, San Francisco, CA 94143, USA

Supplementary data: Supplementary data, including full experimental descriptions of compound synthesis, model descriptions and tables of actual and predicted activities and additional compounds, associated with this article can be found, in the online version.

1. Introduction

Advanced clear cell renal cell carcinoma (RCC) is a disease typified by an aggressive phenotype and poor treatment outcomes.[1,2] Mutation or inactivation of the von Hippel-Lindau (VHL) tumour suppressor gene occurs in the majority of RCCs,[3,4] and this is associated with tumour growth and invasiveness, resulting in a poor prognosis for patients. This gene encodes an E3 ubiquitin ligase that specifically regulates the protein stability of the Hypoxia-Inducible Factor (HIF) family of transcription factors.[5] Loss of VHL results in constitutive expression of HIF leading to increased transcription of genes involved in metabolism, angiogenesis, invasion, metastasis, and proliferation leading to an aggressive phenotype.[6–10] VHL is also known to be involved in a variety of HIF-independent processes.[11–14]

We recently used a synthetic lethality approach[15,16] to identify the *p*yridyl *a*nilino *t*hiazole (PAT) chemotype **1** by high-throughput screening of commercial libraries (Figure 1A). The initial lead **2** was validated as a selective cytotoxin to VHL-deficient cells using XTT growth inhibition and clonogenic survival assays.[17] As well as being selectively cytotoxic to VHL-deficient cells in vitro, compound **2** reduced VHL-deficient RCC growth in a xenograft tumor model in vivo. We demonstrated that the PATs cytotoxicity occurs in a HIF-independent manner through autophagy, however, the molecular target of the PAT class remains unknown. Induction of autophagy to selectively kill tumor cells represents a novel approach to anti-cancer therapy.[18,19]

An initial exploration of structure-activity relationship (SAR) studies was carried out with the synthesis of a range of analogues bearing substitutions on each ring of the PAT chemotype as well as modifications of the linker units between the domains.[20] A quantitative analysis of the SAR was used to determine a possible bioactive conformation for the PAT analogues using Comparative Molecular Field Analysis (CoMFA).

We now report further SAR studies in order to identify more potent and selective PAT analogues with increased potency and selectivity for VHL-deficient RCC. The in vitro activity of PATs as VHL-selective cytotoxins was evaluated using paired RCC cell lines; VHL-deficient RCC4 cell line and the matched line, RCC4-VHL, with the VHL function restored. Two features indentified in the original CoMFA contour maps are explored in this study (Figure 1B). The first feature is the orientation of the thiazole B-ring and the roles of the heteroatom substituents, while the second feature is the positive steric contour (green volume) adjacent to the pyridine ring 3-position which has a nearby disfavored electrostatic red region. We first investigated the influence of thiazole orientation predicted by the alignment model on the biological activity by replacing the thiazole central ring with various heterocycles (**3**–**13**). We then explored the steric region adjacent to the pyridine ring with a range of PAT derivatives bearing various functionalities at the 2- and 3-positions (compounds **14**–**54**) of the pyridine ring. We also report on the impact of additional SAR data on the CoMFA model and compare its predictive ability to that of a 2D-QSAR method, Hologram QSAR (HQSAR).[21]

2. Results

2.1. Chemistry

The thiazole ring was replaced by a range of other 5-membered ring heterocycles. The imidazole analogue **3** was synthesized by condensation[22] between bromoketone **55**[20] and 3-methylphenylguanidinium nitrate **56**[23] using KOH as base (Scheme 1). Similarly, condensation of bromoketone **55** and 3-methylphenylurea **57** afforded oxazole **4**. Thiadiazole derivative **5** was synthesized from 4-pyridinecarbonitrile which was converted

to the corresponding amidine **58** by treatment with NaOMe followed by NH_4Cl addition. Subsequent DIAD-induced heterocyclization of amidine **58** with 3-methylphenylisothiocyanate gave thiadiazole **5**. Methylation of thiourea **59**,[20] gave thiocarbamate **60** which underwent condensation with 4-pyridinecarbohydrazide to give triazole **6** as a mixture of regioisomers. Addition of $MeNH_2$ to 3-methylphenylisothiocyanate gave methylated thiourea **61** which was converted to thiocarbamate **62** by alkylation with MeI, and subsequent condensation with 4-pyridinecarbohydrazide afforded triazole **7**. 3-Methylphenylisothiocyanate was converted to the corresponding hydrazinecarbothioamide **63** by treatment with hydrazine hydrate in EtOH and subsequent condensation with isonicotinic acid in the presence of EDCI gave oxadiazole **8**.

A series of 6-membered ring heterocyclic or carbocyclic analogues were then prepared to further investigate the geometry of the central B ring (Scheme 2). Pyrimidinamine **9** was prepared by condensation of the enaminoketone **64**, obtained by reaction of **4**-acetylpyridine with DMF-DMA, and subsequent reaction with guanidinium nitrate **56** in the presence of KOH.[24] The 2,6-pyrimidine derivative **10** was synthesized from 2,6-dichloropyrimidine by Suzuki cross-coupling reaction with 4-pyridineboronic acid to afford chloropyrimidine **65**, which was reacted with *m*-toluidine under Buchwald conditions to give pyrimidine **10**. The pyrazine **11** and pyridine analogues **12** were prepared using similar synthetic routes. Suzuki reaction of 3-bromoaniline and 4-pyridineboronic acid gave intermediate **68**, which underwent Buchwald reaction with *m*-bromotoluene to give the carbocyclic analogue **13**.

We had previously demonstrated that the introduction of small, lipophilic moieties at the 2- and 3-position was tolerated, while 3-aryl (e.g., 3-Ph-4-Ac **27**) were selective and 3-acetylenic groups (e.g., 3-$C{\equiv}CH_2OMe$ **29**) gave increased potency without lowering selectivity leading to the positive CoMFA derived contour.[20]

To further explore this positive contour we initially targeted a series of fused heteroaryl rings (**14-17**, Scheme 3). Quinoline analogue **14** was prepared from quinoline-4-carboxylic acid which was converted to the corresponding Weinreb amide **69** by reaction with oxalyl chloride followed by treatment with *N, O*-dimethyl hydroxylamine. Subsequent Grignard reaction with MeMgBr to the ketone **70**, then bromination with Br_2/HBr gave the bromoketone **71** which underwent condensation with thiourea **58** to afford **14**. Quinoline **15** was synthesized from 2-phenylquinoline-4-carboxylic acid by conversion to the acid chloride then treatment with $TMSCH_2N_2$ and the intermediate diazoketone was reacted with HBr to give the bromoketone **72**, which was condensed with **58** to give **15**. Imidazopyridine **16** was synthesized by bromination of methylimidazopyridinyl ethanone with Br_2/HBr to give the bromoketone intermediate **72** and subsequent condensation with thiourea **58**. Ketone **74**, prepared by 1,3-dipolar cycloaddition reaction of 3-butyn-2-one and 1-aminopyridinium iodide,[25] was treated with Br_2/HBr to give bromoketone **75** which was condensed with 3-methylphenylthiourea to provide pyrazolopyridine **17**.

Two sets of 3- and 2-substituted pyridyl analogues (**18**–**38** and **39**–**54**, respectively) were then synthesized to further explore the positive contour adjacent to the pyridine ring (Scheme 4). These were obtained by functionalization of the pyridine ring, starting with halopyridines (**76**–**78**)[20] that were further elaborated using Pd-catalyzed Suzuki and Sonogashira cross-coupling reactions (in the case of bromo and iodo compounds) as well as nucleophilic substitution. In some instances, 3-iodopyridine **79**, conveniently prepared from 3-bromopyridine **76** by Cu-catalyzed halogen exchange in the presence of NaI, was used due to the low reactivity of the corresponding 3-bromopyridine **76**. Halopyridines (**76, 77, 79**) were reacted with a series of aryl boronic acids or boronate esters in the presence of $PdCl_2$(dppf) to afford the Suzuki products **18**–**27** and **39**–**49**. Sonogashira reactions of 3-

bromopyridine **76** with propargyl alcohol, methyl propargyl ether, 1-butynol and 1-pentynol, using $PdCl_2(PPh_3)_2$ and CuI as catalysts gave compounds **28, 29, 30** and **31**, respectively. The terminal hydroxyl group was also replaced with polar amine groups to increase aqueous solubility. Boc protection of **76** using Boc_2O in DCM gave bromide **80** which underwent Sonogashira cross-coupling with 1-butynol to produce intermediate alcohol **81** which was further functionalized by treatment with MsCl, displacement with morpholine or *N*-methylpiperazine, and removal of the Boc group with TFA to give analogues **32** and **33**.

Triazole analogues **34** and **50** were synthesized using "Click" chemistry. Sonogashira cross-coupling reactions between bromides **76** and **77** and TMS acetylene in the presence of $PdCl_2(PPh_3)_2$ and CuI, followed by removal of the TMS group using K_2CO_3 gave acetylenes **82** and **83**.[20] Reaction of **82** and **83** with benzyl azide in the presence of copper sulfate and sodium ascorbate gave benzyltriazole analogues **34** and **50**, respectively.

In an effort to explore whether a flexible linker could access the steric contour as effectively as the equivalent soluble acetylenes **32** and **33**, a range of alkylamines linked at the 2- and 3-positions via nitrogen and oxygen linker atoms were prepared. Nucleophilic substitution of 3-fluoropyridine **78** and 2-bromopyridine **77** with *N*-methylpiperazine, 2-morpholinoethanamine, 2-morpholinoethanol, and 3-(dimethylamino)-1-propanol gave the derivatives **35**–**38** and **51**–**54**, respectively.

2.2. Biological assays

Cellular growth inhibition was determined by IC_{50} assays, using a 4-day drug exposure of RCC4 and RCC4/VHL cells in 96-well plates as described previously.[17] The selectivity ratio was calculated as the intraexperiment ratio IC_{50}(RCC4/VHL)/IC_{50}(RCC4) (Tables 1–4). Several active analogues were also examined for their ability to induce formation of intracytoplasmic vacuoles to indicate whether they were killing cells by the induction of autophagy. Cells were incubated with drug (5 μM) for 24 h before phase contrast images were taken (Figure 3).

2.3. Molecular modeling

We previously reported a CoMFA derived 3D-QSAR model that accounted for 34% (q^2 = 0.344) of the variation in the selective cytotoxicity of the PAT series against a VHL deficient renal cell line, and provided a putative bioactive conformation for this compound series.[20] This model (Figure 1B) was recreated by molecular alignment of the compound training set previously described against **28** (Table 4, Model 1) and differs marginally from that previously published. Here we examine the effect of new PAT analogues on this model (Table 4).

Incorporating Table 1 compounds of defined IC_{50} into Model 1 generated Model 2, and had a negative effect on the base model, reducing the q^2 from 0.352 to 0.27. Two conformers for each of **14**–**16** (Table 2) were assessed against Model 1, these conformers explored different orientations of the pyridyl A-ring substitutions, and the orientations with the best q^2 values were used to build Model 3, giving results similar to Model 1. Including 2-pyridyl substituents in model 1 had a negative effect on q^2, decreasing it from 0.352 (Model 1) to 0.246 (Model 4), 3-pyridyl substituents improved q^2 (0.423 vs 0.352). A set of compounds was then selected across all substitution patterns that, along with those used in Model 1, represent the complete PAT training set, and give Model 6 (See Supplementary data for composition of the training set). The q^2 of this model was comparable, albeit slightly reduced, to Model 1 at 0.313, and is only able to account for 31% of the variance in biological activity.

As one of the most important characteristics of a QSAR model is its ability to predict a target property for molecules not used in its development, the ability of Model 6 to predict IC_{50} values was tested against an external test set of compounds generated from Tables 1–3 along with additional compounds (from Reference 20) not used in the construction of Model 1 (Supplementary data, Table S1). Many of these compounds either displayed low activity, had IC_{50} values >40 μM, side chain substitutions with more than 1 rotatable bond, or unknown activity. Model 6 showed a linear relationship between experimental and predicted IC_{50} values for the training set with a non-validated r^2 of 0.89, Standard Error of Estimation of 0.18 (Table 4 and Supplementary data, Figure S1), and a maximum difference between actual and predicted values (residual) of 0.44 (Supplementary data, Table S2A). While the log activity range of the Model 6 training set ranged from 4.3 to 6.7, most compounds (82%) were in the smaller range of 4.5 to 6 and this may contribute to the low q^2 value. Comparison of actual and predicted activities for the test set does not show any correlation ($r^2 = 0.07$) (Supplementary data, Figure S1), and many compounds with IC_{50} values >40 μM are incorrectly predicted, although an r^2 of 0.10 when these compounds are excluded also indicates an absence of correlation for the remainder of the test set with defined IC_{50} values. The residual values ranged from 0.01 to 1.77 with approximately 55% of the test set predicted within 0.45 log units, the maximum residual value observed for the training set, and 60% predicted within 0.5 log units (Supplementary data, Table S2B). This low predictivity is consistent with the low q^2 value. The CoMFA generated contour maps are illustrated in Figure 2.

To determine if the CoMFA model was limited by the alignment strategy, a 2D-QSAR analysis was also performed using HQSAR.[21] As HQSAR models are influenced by fragment size and distinction, a series of models were generated using a range of parameters (Table 5). Model 12 was the best fragment distinction combination, with a q^2 of 0.361, and this was slightly improved to 0.375 when the fragment length was increased (Table 6, model 26 versus model 30). Interestingly, HQSAR Model 30 showed a reduced correlation between actual and predicted values compared to the CoMFA Model 6, while the Standard Error was slightly higher. The maximum difference between experimental and predicted activities for the training set was 0.58 (Supplementary data, Table S3A). External validation of Model 30 did not show any correlation between predicted and actual activities (r^2=0.0009), and many compounds with poor activity (IC_{50} >40 μM) were incorrectly predicted (Supplementary data, Figure S2), and the r^2 was not improved when these compounds were excluded. The residual values ranged from 0.06 to 1.44 with approximately 60% of the test set predicted within 0.58 log units, the maximum residual value observed for the training set (Supplementary data, Table S3B) and the range in difference outside this cutoff was 0.60 to 1.44.

3. Discussion

A putative bioactive 3-dimensional conformation of the PAT series identified by CoMFA was used to guide synthesis of a set of PAT analogues which were designed to explore the central B-ring and its role in the alignment of the molecule and to probe the nature of the steric pocket adjacent to the pyridine A-ring. Previous exploration of the basic SAR around the aniline C-ring had shown that small, lipophilic substituents were optimal for activity hence we chose to use the 3-methylaniline ring.[20]

The ligand model gave a consistent curved orientation with the thiazole *N* placed in the inner surface and the thiazole *S* on the exposed rim (Figure 2). Replacement of the thiazole ring with any other 5-membered-ring heterocycle led to either a large drop in potency and selectivity or complete loss of activity (Table 1). Replacement of the thiazole S with another heteroatom (NH and O) led to inactive analogues (**3** and **4**). Incorporation of an additional *N*

within the central ring gave much less potent derivatives (e.g., thiadiazole **5**) while retaining a hint of selectivity, although lack of aqueous solubility prevent a full determination in the RCC4/VHL cell line (Table 1). Similarly, triazole analogues displayed low potency and selectivity. It was not possible to fully evaluate the influence of the thiazole *N* on the biological activity as our efforts towards the synthesis of a thiophene analogue were unsuccessful with the instability of the desired thiophene product precluding purification. We compared the effect of the substitution of *O* for *S* by overlaying minimised structures of thiazole **2**, oxazole **4** and thiadiazole **8** and noted that only a small conformational shift was seen in the case of the oxazole (Supplementary data, Figure S3).

Evaluation of the 6-membered ring analogues showed that introduction of a phenyl ring totally abolished selectivity (e.g., **13**). Retention of an *N*-atom in the 2-position of the central ring was necessary for activity against the VHL-deficient RCC4 line (e.g., **9, 11, 12**), although it was not sufficient for selectivity with pyrimidine **9** being nonselective. There was no correlation between the pKa of either the pyridyl N, or the aniline NH, and cytotoxic potency across the series **1**–**13**. Taken together, it seems likely that the thiazole *N* plays a key role in the binding to the target; isosteric replacement of the thiazole *S* with =CH is tolerated in six-membered rings, but other minor modifications of the central ring result in a loss in potency, thus these analogues were not pursued further.

The putative space around the pyridine ring was explored with analogues bearing fused rings to provide an extended aromatic region. We had previously demonstrated[20] that a 4-pyridine was the only regioisomer that retained activity and so the heterocycles were designed to place an *N*-atom in a similar spatial location. These rigid, bulky aromatic systems generally gave low potency and selectivity (Table 2), suggesting that optimising the steric interaction might require a more directed approach.

Hence, a set of aryl, alkynyl alkyloxy and alkylamino analogues were synthesized by elaboration of the pyridine with a variety of functional groups conveniently introduced by use of Suzuki and Sonogashira reactions, Click chemistry, as well as direct nucleophilic displacement of aryl halides. Functionalization of the pyridine at the 3-position was examined first with simple aryl **18** and pyridyl **19** substituents resulting in decreased potency and selectivity relative to **2**. Addition of a range of lipophilic substituents at the 4-position of the phenyl group (**20**–**27**) gave a range of activities and suggested the potential for a lipophilic **H**-bond acceptor such as sulphone **25** or methyl ketone **27** to provide potency in the low micromolar range and modest selectivity. In contrast, more polar **H**-bond acceptor/donor carboxamides **22** and **24** were less potent and non-selective.

We had previously demonstrated the 3-propargyl analogues **28** and **29** displayed increased potency while maintaining selectivity,[20] thus the higher homologues **30** and **31** were prepared. However, increasing alkyl chain length was not favourable and resulted in decreasing potency and selectivity and increasing the terminal bulk was also disfavoured, with only the morpholine **32** being comparable to **28** and **29**. Incorporation of the benzyltriazole unit **34** abolished activity.

Pyridines bearing flexible solubilising basic amine side chains generally retained potency but displayed low selectivity (e.g., **35**–**38**). Curiously, the oxygen-linked amines **37** and **38** were superior to the nitrogen-linked amines **35** and **36**. The data on the 3-series show that while substituted phenyl groups at the 3-position of the pyridine gave some active compounds, the most potent analogues were obtained with the introduction of a small H-bond acceptor (e.g., CH_2OH, CH_2OMe) linked *via* a rigid acetylene.

We finally examined substitutions at the 2-position of the pyridine to see if these could also provide positive steric interactions. In contrast with the 3-series, use of a variety of 6-

membered rings (**40**–**44**), gave compounds with low potency and selectivity. Interestingly, the introduction of a range of 5-membered ring heterocycles (**45**–**50**) gave analogues that generally were active and selective with the only anomaly being the 1-methyl pyrazole **48**. The 1-benzylpyrazole derivative **49** had low micromolar activity and a high selectivity ratio of **30**, which was similar to the benzyltriazole analogue **50**, whereas the unsubstituted pyrazole analogue **47** showed a four-fold increase of potency while preserving a modest selectivity of 14-fold. Together the data suggests the presence of a second domain adjacent to the 2-position of the pyridine ring which can accommodate a five-membered ring. The exact definition of this domain and the associated H-bond contacts remain to be fully characterized. Introduction an alkyl chain at the 2-position with solubilising tertiary amines gave compounds (**51**–**54**) with low selectivity.

A series of active compounds (**2, 32, 38, 47**, and **49**) were examined to confirm that the mechanism of cell death involved the induction of autophagy. Treatment of RCC4 cells with 5 μM of each drug for 24 h induced the formation of intracytoplasmic vesicles confirming VHL-selective induction of autophagy resulting in cell death (Figure 3).

CoMFA was used with the data from this and an earlier study to better understand the effects of substitutions around the PAT core on activity. The 3D-QSAR model generated could only explain approximately 30% of the variance in the IC_{50} data, and this was reflected in its lack of predictivity of an external test set of compounds. A similar result was also found when a 2D-QSAR method (HQSAR) was used, indicating that the alignment strategy used to generate the CoMFA model was appropriate, and that the SAR data of the PAT series with respect to autophagy may be quite complex.

Examination of the CoMFA contour maps generated from Model 6 using the complete training set (Figure 2) shows that, within the training set, the contouring around the aniline C-ring is similar to that previously published. The new PAT CoMFA model exhibits a large region adjacent to the sulfur of the thiazole B-ring of **28** that suggests a positive electrostatic effect will favor activity. Interestingly, this region has three distinct, yet interconnected regions. Two of these are found around either side of the B-ring while the third is more accessible by substitution from the pyridyl ring 3-position substitution, as substitutions on this ring were all seen to reduce activity. Around the pyridyl group, increased steric bulk is positively associated with activity around the 2- and 3-positions, consistent with the previous model. From the compounds characterized in Table 3, this region is better accessed by substitutions at the 3-position as suggested by the higher potency across a number of homologues. Two distinct regions around the pyridyl 2-position and nitrogen atom indicate contrasting effects of steric bulk on activity. A region adjacent to the 2-position indicates that increased steric bulk is associated with decreased activity (yellow contour); although this is contrasted by the 2-pyrazole that has increased bulk at this position yet has the strongest activity recorded for a 2-position substitution. This region of disfavored steric bulk is also accessed by the fused ring compounds (Table 2) e.g. **15**. The pyrazole moiety may contribute to an additional favorable steric bulk zone adjacent to the N-atom (green contour).

The further development of the CoMFA alignment model has not produced gains in the ability of the model to explain the QSAR observed. Despite generating six different models we are unable to explain more than 31% of the variance observed and did not significantly improve on this using the alternative HQSAR approach. This low predictivity may be a consequence of the complexity of the phenotypic readout which reports the product of many combined parameters rather than just the interaction of the PAT with the molecular target. Although we have further explored the SAR around the pyridyl A-ring and B-ring, the relatively small gains in potency and selectivity seen with the 2- and 3-substituted pyridyl

analogues, coupled with the relatively flat SAR profile observed in our previous study, suggest that the PAT series may occupy a local minimum and a large random leap may be necessary to improve potency and selectivity substantially. We will endeavour to use the alignment model generated in this study to conduct a virtual screen in an effort to identify new chemotypes with VHL-selective activity. In another approach, we plan to exploit the steric tolerance adjacent to the pyridyl ring to introduce linker moieties to assist in the preparation of molecular probes to isolate and identify the molecular target of this PAT chemotype.

4. Experimental Section

Chemistry 4.1

4.1.1. General method A. Suzuki reaction of 2,6-dichloropyrimidine, 2,6-dichloro pyrazine, 2,6-dichloropyridine and 3-bromoaniline (Compounds 65–68)—Boronic acid or ester (10.0 mmol), K_2CO_3 (25.0 mmol) in H_2O (10 mL) and $Pd(PPh_3)_4$ (0.3 mmol) were added sequentially to a solution of aryl halide (10.0 mmol) in 1,4-dioxane (40 mL). The reaction mixture was stirred at 90 °C for 2–20 h and was then cooled to 20 °C and partitioned between EtOAc (200 mL) and H_2O (100 mL). The organic phase was washed with water (3 × 50 mL), washed with brine (50 mL), dried and the solvent was evaporated. The residue was purified by column chromatography, eluting with an appropriate gradient of EtOAc/pet. ether, to give the Suzuki product.

4.1.2. General method B. Buchwald reaction (Compounds 11–13)—$Pd(OAc)_2$ (0.37 mmol), BINAP (0.37 mmol) and NaO*t*Bu (10.30 mmol) were sequentially added to a stirred, degassed solution of aryl halide (3.68 mmol) and amine (7.36 mmol) in a mixture of toluene (50 mL) and DMF (5 mL) and the mixture was heated at 90 °C for 4–5 h. The mixture was cooled to 20 °C, diluted with Et_2O (200 mL), washed with water (3 × 50 mL), washed with brine (50 mL), dried and the solvent was evaporated. The residue was purified by column chromatography, eluting with an appropriate blend of EtOAc/pet. ether, to give the Buchwald product.

4.1.3. General method C. Preparation of pyridyl 2-bromoethanones (Compounds 71, 73, 75)—Br_2 (80 mmol) was added dropwise to a stirred solution of acetylpyridine (80 mmol) in 30% HBr/HOAc (100 mL) at 15 °C. The mixture was stirred at 40 °C for 1 h and then 75 °C for 1 h. The mixture was cooled to 20 °C, diluted with Et_2O (400 mL) and stirred for 30 min. The precipitate was filtered, washed with Et_2O (25 mL) and dried under vacuum to give the bromoethanone as the hydrobromide salt.

4.1.4. General method D. Preparation of thiazoles (Compounds 14–17)—A mixture of bromoketone hydrobromide (3 mmol) and phenylthiourea (3 mmol) in EtOH (20 mL) was stirred at reflux temperature for 1 h. The mixture was cooled to 20 °C, diluted with water (50 mL), the pH adjusted to ca. 8 with aqueous NH_3 and the mixture stirred at 20 °C for 2 h. The precipitate was filtered, washed with water (5 mL) and dried. The solid was purified by column chromatography, eluting with an appropriate blend of EtOAc/pet. ether, to give the thiazole.

4.1.5. General method E. Suzuki reactions with bromo- and iodopyridines (Compounds 18–27 and 39–49)—$PdCl_2$(dppf) (0.03 mmol) was added to a stirred, degassed solution of bromo- or iodopyridine (0.29 mmol), boronic acid or ester (0.45 mmol) and K_2CO_3 (3.00 mmol) in a mixture of toluene/EtOH/H_2O/DMF (5:3:1.5:4, 13.5 mL) and the mixture was heated at 90 °C for 16 h. After cooling to 20 °C, the mixture was partitioned between EtOAc (100 mL) and water (50 mL), the combined organic phase was washed with

H_2O (3 × 50 mL), washed with brine (50 mL), dried and the solvent was evaporated. The residue was purified by column chromatography, eluting with an appropriate blend of EtOAc/pet. ether or aqueous NH_3/MeOH/DCM, to give the Suzuki product.

4.1.6. General method F. Sonogashira reactions with bromopyridine (Compounds 30, 31 and 81)—$PdCl_2(PPh_3)_2$ (0.03 mmol) was added to a stirred, degassed solution of bromopyridine (0.58 mmol), alkyne (0.70 mmol) and CuI (0.03 mmol) in a 1:1 mixture of DMF and NEt_3 (4 mL), and the reaction mixture was stirred at 50 °C for 16 h then at 70 °C for 4 h. After cooling to 20 °C, the mixture was partitioned between EtOAc (150 mL) and water (50 mL), the organic phase was washed with water (3 × 50 mL), washed with brine (50 mL), dried and the solvent was evaporated. The residue was purified by column chromatography, eluting with an appropriate blend of EtOAc/pet. ether, to give the alkyne.

4.1.7. General method G. Elaboration of propargyl alcohol (Compounds 32 and 33)—MsCl (0.28 mmol) was added to a solution of alcohol **81** (0.24 mmol) and NEt_3 (0.36 mmol) in anhydrous DCM (10 mL) at -20 °C and the reaction mixture was stirred at -20 °C for 1 h. The mixture was diluted with DCM (100 mL), washed with water (3 × 50 mL), washed with brine (50 mL), dried and the solvent was evaporated. Amine (2.4 mmol) was added to a solution of the crude mesylate in anhydrous THF (5 mL), and the mixture was heated at 50 °C for 2 h. The mixture was cooled to 20 °C, partitioned between EtOAc (100 mL) and water (50 mL), the organic layer was washed with aqueous $NaHCO_3$ (50 mL), washed with brine (50 mL), dried and the solvent was evaporated. A mixture of crude carbamate in DCM (10 mL) and TFA (1 mL) was then stirred at 20 °C for 1 h. The solvent was evaporated and the residue was purified by column chromatography, eluting with appropriate blend of aqueous NH_3/MeOH/DCM, to give the alkyne.

4.1.8. General method H. Click reaction (Compounds 34 and 50)—$CuSO_4 \cdot 5H_2O$ (0.02 mmol) and sodium ascorbate (0.04 mmol) were added to a solution of acetylene (0.18 mmol) and benzyl azide (0.20 mmol) in a 1:1:1 mixture of DCM/EtOH/H_2O (3 mL), and the mixture was stirred at 20 °C for 20 h. The mixture was partitioned between EtOAc (100 mL) and water (50 mL), extracted with EtOAc (2 × 70 mL), the combined organic phase was washed with water (2 × 30 mL), washed with brine (30 mL), dried and the solvent was evaporated. The residue was purified by column chromatography, eluting with an appropriate blend of MeOH/DCM, to give the triazole.

4.1.9. General method I. Fluoride and bromide displacement reactions (Compounds 35–38 and 51–54)—A mixture of 3-fluoro or 2-bromopyridine (0.35 mmol) in the appropriate amine or alcohol (2 mL) was heated in a sealed glass pressure vessel at 100–180 °C for 16-24 h (in some cases, the reaction was done in the presence of Cs_2CO_3). The solution was cooled to 20 °C, partitioned between EtOAc (100 mL) and water (50 mL), the organic phase was washed with water (2 × 50 mL), washed with brine (50 mL), dried and the solvent was evaporated. The residue was purified by column chromatography, eluting with an appropriate blend of aqueous NH_3/MeOH/DCM to give the substitution product.

4.2. Cell Viability Assays

For 2,3-bis[2-methoxy-4-nitro-5-sulfophenyl]-2H-tetrazolium-5-carboxanilide (XTT) assays, five thousand cells were plated in 96-well plates. The next day, vehicle (DMSO) or drug was added by serial dilution. Four days later the media was aspirated, XTT solution (0.3 mg/ml of XTT (Sigma), 2.65 mg/ml N-methyl dibenxopyrazine methyl sulfate (Sigma) in phenol red-free media) was added, and the plates were incubated at 37 °C for 1-2 hours.

Metabolism of XTT was quantified by measuring the absorbance at 450 nm. IC_{50} values were calculated using linear interpolation.

4.3. QSAR modeling

4.3.1. Alignment Generation—A minimum energy conformation of **2** was generated using OMEGA2 (Openeyes Software, USA) with default parameters using the MMFF94s force field and the rms torsion driving parameter set at 0.6. All other structures were generated from this conformation using the SKETCHER (SYBYL8.0, TRIPOS) and minimised using MAXMIN2 (SYBYL8.0) with the Tripos Force field and Gastieger-Huckel charges. Minimisation was performed using 1000 steps of steep decents followed by conjugate gradients until convergence at 0.05 kcal/(molÅ). A distance dependent dielectric function was used with a dielectric constant of 80. Molecular alignments were generated by superimposition of all compounds onto **28** using ROCS (Openeye Software, USA) with default parameters using both the shape only and shape in combination with color force field method. While the shape only alignment was used for CoMFA, those compounds poorly aligned as assessed after visual inspection, were replaced by improved alignments from the shape and colour force field combination alignment if available. Alternate proton positions were explored for compound **6**, while alternative conformers based on rotating the B-ring relative to the C-ring were also explored.

4.3.2. 3D-QSAR Analysis—CoMFA was used to determine a relationship between the compounds tested and *in vitro* cytotoxicity as previously described.[20] The SAMPLS Leave One Out (LOO) protocol was used to determine the cross-validated r^2 (q^2) as a indicator of the predictivity of the 3D-QSAR model along with the optimum number of components, which was subsequently used in a conventional non-validated PLS analysis. Only compounds that had defined IC_{50} data and cytotoxicity ratios, and substitutions including up to one rotatable bond were used. A base CoMFA 3D-QSAR model was created using a previously described compound set (Model 1)[20] and compounds from each substitution pattern were added into this generating Models 2-5, and a compound set representing all PAT analogues was used to generate Model 6. The compound sets used to generate each model are listed in the Supplementary data.

4.3.3. 2D-QSAR Analysis—The 2D-Hologram QSAR (HQSAR) method[21] as implemented in SYBYL×1.2 was used to eliminate any dependency of the CoMFA QSAR model on compound 3D structure, conformation and alignment strategy. In this method each compound is broken down into all possible linear, branched and cyclic structural fragments and these are counted into arrays of fixed length, a molecular hologram. The bin occupancies associated with the molecular hologram are descriptor variables that can be related to biological activity by Partial Least Squares analysis. As HQSAR models can be affected by hologram length, fragment size and distinction, a series of models characterising variation in these parameters were generated to find the optimal QSAR model for the PAT series as determined by the highest q^2 value. Using the default fragment size of 4–7 atoms, the effect of different fragment distinctions on q^2 was explored. The optimal fragment distinction combination was then used to characterise the effect of fragment size on HQSAR model q^2.

Supplementary Material

Refer to Web version on PubMed Central for supplementary material.

Acknowledgments

The authors thank Dr Maruta Boyd, Dr Shannon Black, Stefanie Maurer and Sisira Kumara for technical assistance and acknowledge the Association for International Cancer Research 10-0042 (MB), the Maurice Wilkins Centre for Biodiscovery (MPH, JUF), US NCI-CA-82566 (AJG, MPH), NCI-CA-123823 (DAC), NCI-T32-CA-121940 (EWL) for funding.

References and notes

1. Motzer RJ, Mazumdar M, Bacik J, Berg W, Amsterdam A, Ferrara J. J Clin Oncol. 1999; 17:2530. [PubMed: 10561319]
2. Murai M, Oya M. Curr Opin Urol. 2004; 14:229. [PubMed: 15205579]
3. Gnarra JR, Tory K, Weng Y, Schmidt L, Wei MH, Li H, Latif F, Liu S, Chen F, Duh FM, Lubensky I, Duan DR, Florence C, Pozzatti R, Walther MM, Bander NH, Grossman HB, Brauch H, Pomer S, Brooks JD, Isaacs WB, Lerman MI, Zbar B, Linehan WM. Nature Genet. 1994; 7:85. [PubMed: 7915601]
4. Kim WY, Kaelin WG Jr. J Clin Oncol. 2004; 22:4991. [PubMed: 15611513]
5. Maxwell PH, Wiesener MS, Chang GW, Clifford SC, Vaux EC, Cockman ME, Wykoff CC, Pugh CW, Maher ER, Ratcliffe PJ. Nature. 1999; 399:271. [PubMed: 10353251]
6. Gnarra JR, Zhou S, Merrill MJ, Wagner JR, Krumm A, Papavassiliou E, Oldfield EH, Klausner RD, Linehan WM. Proc Natl Acad Sci USA. 1996; 93:10589. [PubMed: 8855222]
7. Iliopoulos O, Levy AP, Jiang C, Kaelin WG Jr, Goldberg MA. Negative regulation of hypoxia-inducible genes by the von Hippel-Lindau protein. Proc Natl Acad Sci USA. 1996; 93:10595. [PubMed: 8855223]
8. Knebelmann B, Ananth S, Cohen HT, Sukhatme VP. Cancer Res. 1998; 58:226. [PubMed: 9443397]
9. Staller P, Sulitkova J, Lisztwan J, Moch H, Oakeley EJ, Krek W. Nature. 2003; 425:307. [PubMed: 13679920]
10. Erler JT, Bennewith KL, Nicolau M, Dornhofer N, Kong C, Le QT, Chi JT, Jeffrey SS, Giaccia AJ. Nature. 2006; 440:1222. [PubMed: 16642001]
11. Ohh M, Yauch RL, Lonergan KM, Whaley JM, Stemmer-Rachamimov AO, Louis DN, Gavin BJ, Kley N, Kaelin WG Jr, Iliopoulos O. Mol Cell. 1998; 1:959. [PubMed: 9651579]
12. Hergovich A, Lisztwan J, Barry R, Ballschmieter P, Krek W. Nat Cell Biol. 2003; 5:64. [PubMed: 12510195]
13. Okuda H, Saitoh K, Hirai S, Iwai K, Takaki Y, Baba M, Minato N, Ohno S, Shuin T. J Biol Chem. 2001; 276:43611. [PubMed: 11574546]
14. Na X, Duan HO, Messing EM, Schoen SR, Ryan CK, di Sant'Agnese PA, Golemis EA, Wu G. EMBO J. 2003; 22:4249. [PubMed: 12912922]
15. Kaelin WG Jr. Nature Rev Cancer. 2005; 5:689. [PubMed: 16110319]
16. Chan DA, Giaccia AJ. Cell Cycle. 2008; 7:2987. [PubMed: 18818511]
17. Turcotte S, Sutphin PD, Chan DA, Hay MP, Denny WA, Giaccia AJ. Cancer Cell. 2008; 14:90. [PubMed: 18598947]
18. Turcotte S, Giaccia AJ. Curr Opin Cell Biol. 2010; 22:246. [PubMed: 20056398]
19. Fleming A, Noda T, Yoshimori T, Rubinstein DC. Nature Chem Biol. 2011; 7:9. [PubMed: 21164513]
20. Hay MP, Turcotte S, Flanagan JU, Bonnet M, Chan DA, Sutphin PD, Nguyen P, Giaccia AJ, Denny WA. J Med Chem. 2010; 53:787. [PubMed: 19994864]
21. Heritage, TW.; Lowis, DR. Molecular Hologram QSAR. In: Parrill, AL.; Reddy, MR., editors. Rational Drug Design Novel Methodology and Practical Applications. Vol. 719. American Chemical Society; Washington, DC: 1999. p. 212-225.ACS Symposium Series
22. Mahboobi S, Sellmer A, Eswayah A, Elz S, Uecker A, Böhmer FD. Eur J Med Chem. 2008; 43:1444. [PubMed: 17983688]
23. Tavares FX, Boucheron SH, Griffin RJ, Preugschat F, Thomson SA, Wang TY, Zhou HQ. J Med Chem. 2004; 47:4716. [PubMed: 15341487]

24. Adams H, Batten SR, Davies GM, Duriska MB, Jeffery JC, Jensen P, Lu J, Motson GR, Coles SJ, Hursthouse MB, Ward MD. Dalton Trans. 2005:1910. [PubMed: 15909037]
25. Miki Y, Nakamura N, Hachiken H, Takemura S. J Het Chem. 1989; 26:1739.

Abbreviations

BINAP	2,2′-bis(diphenylphosphino)-1,1′-binaphthyl
CoMFA	comparative molecular field analysis
DCM	dichloromethane
DIAD	diisopropyl azodicarboxylate
DMF-DMA	dimethylformamide-dimethylacetal
dppf	1,1′-bis(diphenylphosphino)ferrocene
EDCI	1-ethyl-3-(3-dimethylaminopropyl) carbodiimide
HQ-SAR	hologram quantitative structure activity relationship
HIF	hypoxia-inducible factor
PAT	pyridyl anilinothiazoles
VHL	von Hippel-Lindau
RCC	renal cell carcinoma
SAR	structure-activity relationship
XTT	2, 3-bis[2-methoxy-4-nitro-5-sulfophenyl]-2*H*-tetrazolium-5-carboxanilide

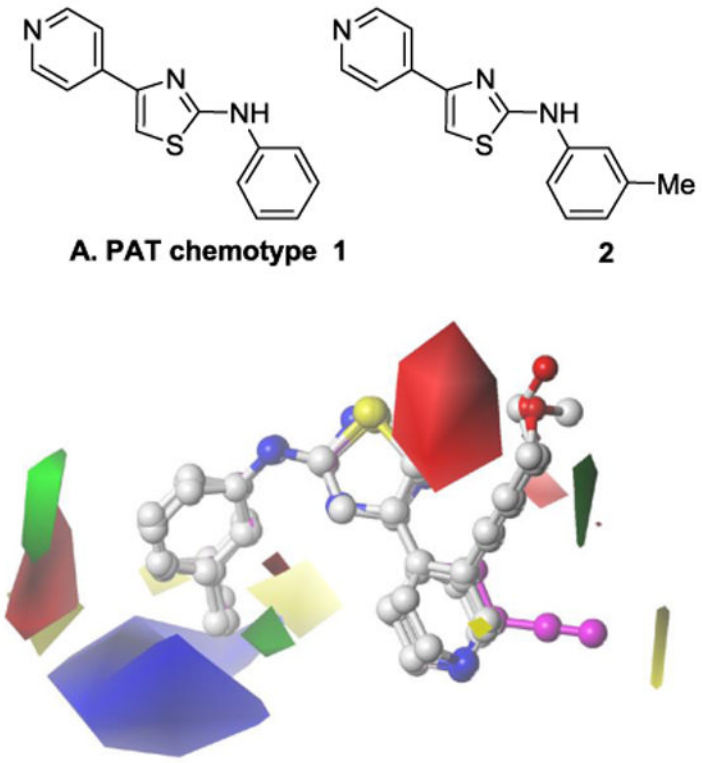

Figure 1. PAT chemotype and biologically relevant alignment

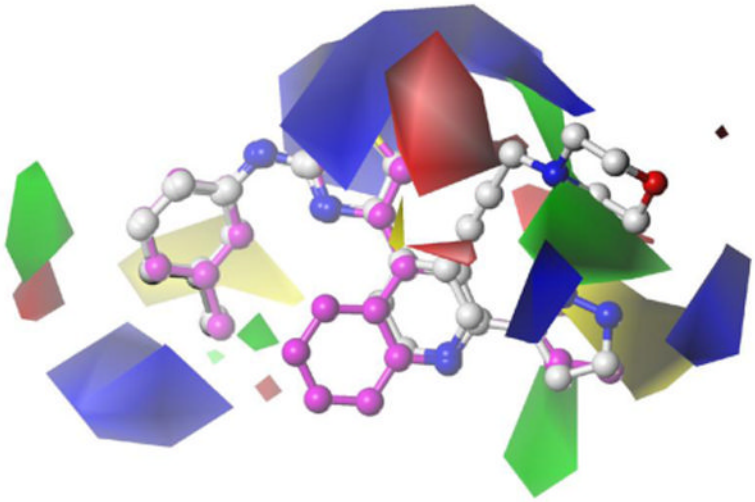

Figure 2. New biologically relevant alignment

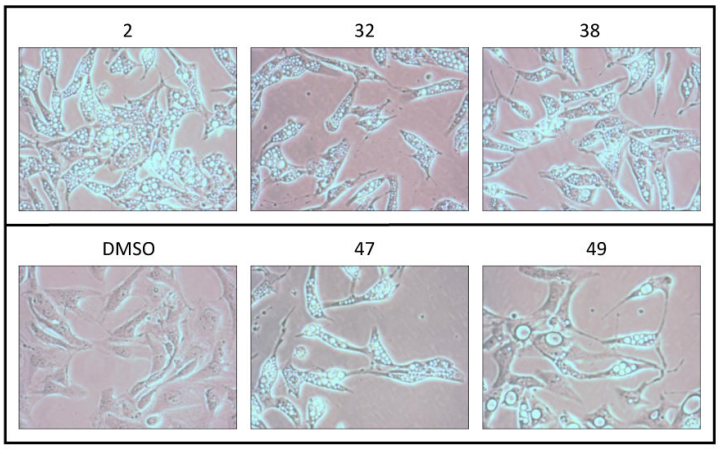

Figure 3.
Induction of Autophagy by PATs in RCC4 Cells [a]
[a] RCC4 cells, 20×, after 5 μM drug exposure for 24 h.

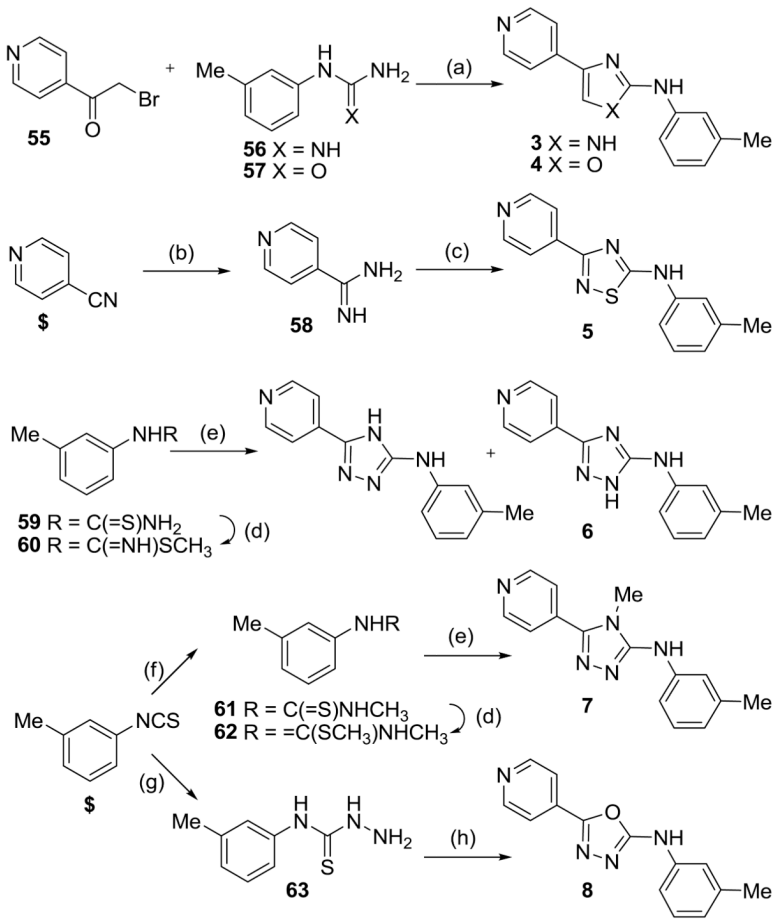

Scheme 1.

Reagents and conditions: (a) KOH, NEt_3, EtOH, 80 °C; (b) NaOMe, MeOH, then NH_4Cl; (c) 3-methylphenyl isothiocyanate, iPr_2NEt, DMF, then DIAD; (d) MeI, EtOH; (e) 4-pyridinecarbohydrazide, pyridine; (f) $MeNH_2$, EtOH; (g) NH_2-NH_2·H_2O, EtOH; (h) isonicotinic acid, EDCI, DCM. $ = commercially available.

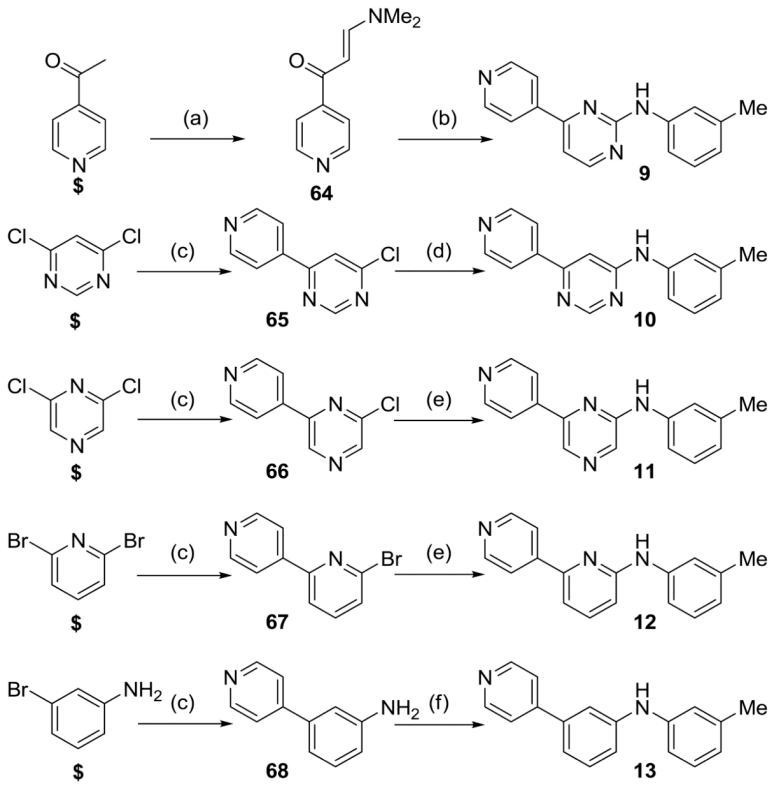

Scheme 2.

Reagents and conditions: (a) DMF-DMA, reflux; (b) **56**, NaOH, iPrOH, reflux; (c) $Pd(PPh_3)_4$, 4-pyridineboronic acid, K_2CO_3, 1,4-dioxane, 80 °C; (d) *m*-toluidine, *p*-TsOH, 1,4-dioxane, reflux; (e) *m*-toluidine, $Pd(OAc)_2$, BINAP, NaO*t*Bu, toluene, DMF, 90 °C; (f) *m*-bromotoluene, $Pd(OAc)_2$, BINAP, NaO*t*Bu, toluene, DMF, 90 °C. $ = commercially available.

Scheme 3.

Reagents and conditions: (a) $(COCl)_2$, DMF, DCM; (b) Me(OMe)NH·HCl, NEt_3, DCM; (c) MeMgBr, THF; (d) Br_2, HOAc/HBr; (e) arylthiourea **58**, EtOH; (f) $TMSCH_2N_2$, THF; then HBr. $ = commercially available.

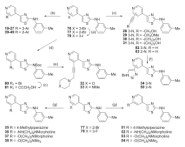

Scheme 4.

Reagents and conditions: (a) CuI, NaI, $H_2N(CH_2)_2NH_2$, 1,4-dioxane, 110 °C; (b) $PdCl_2$(dppf), Ar-boronic acid or ester, K_2CO_3, Tol/EtOH/H_2O/DMF, 90 °C; (c) $PdCl_2(PPh_3)_2$, CuI, HC≡C-R, NEt_3/DMF, 50–70 °C; (d) Boc_2O, DMAP, DCM; (e) i) MsCl, NEt_3, DCM, −20 °C, ii) morpholine or *N*-methylpiperazine, K_2CO_3, DMF, iii) TFA, DCM; (f) $CuSO_4$, Na ascorbate, BnN_3, DCM/EtOH/H_2O, 20 °C; (g) ROH or RNH_2, neat, Cs_2CO_3, 160–180 °C.

Table 1

IC_{50} values and selectivity ratios for B-ring analogues.

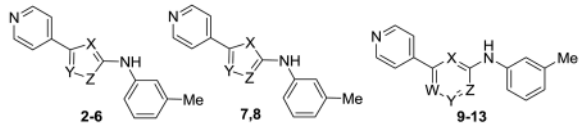

No	X	Y	Z	W	RCC4 IC_{50} μM	RCC4/VHL IC_{50} μM	Ratio[a]
1	N	CH	S		7	>70	>10
2	N	CH	S		2.1	40	19
3	N	CH	NH		>40	>40	ND
4	N	CH	O		>40	>40	ND
5	N	N	S		24.8	>40	>1.6
6	N	N	NH		28.7	22.2	0.8
7	NMe	N	N		>40	>40	ND
8	O	N	N		>40	>40	ND
9	N	CH	N	CH	6.5	8.6	1.3
10	CH	CH	N	N	23.1	28.1	1.2
11	N	N	CH	CH	8.5	31.8	3.7
12	N	CH	CH	CH	7.4	>40	>5.4
13	CH	CH	CH	CH	36.9	38.1	1.0

[a] Ratio = IC_{50} (RCC4/VHL)/IC_{50} (RCC4)

Table 2

IC_{50} values and selectivity ratios for fused A-ring analogues.

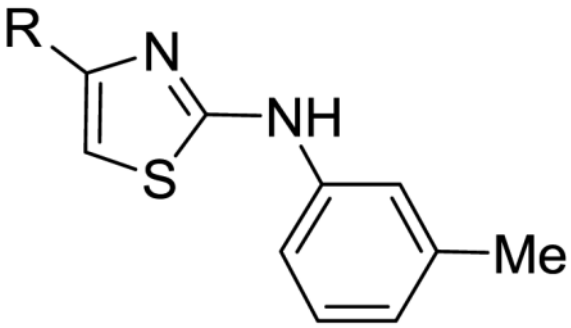

No	R	RCC4 IC_{50} μM	RCC4/VHL IC_{50} μM	Ratio[a]
14	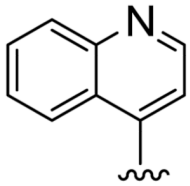	12.3	20.0	1.6
15	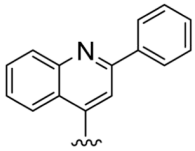	25.4	>40	>1.6
16	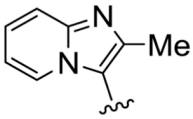	9.5	29.8	3.1
17	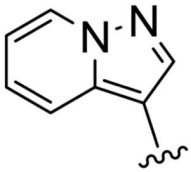	>40	15.3	<0.4

[a] Ratio = IC_{50} (RCC4/VHL)/IC_{50} (RCC4)

Table 3

IC_{50} values and selectivity ratios for substituted A-ring analogues.

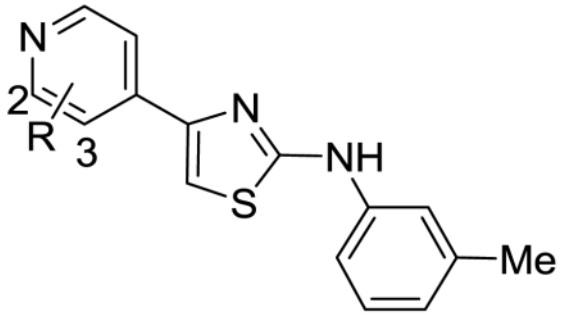

No	3-R	RCC4 IC_{50} μM	RCC4/VHL IC_{50} μM	Ratio[a]	No	2-R	RCC4 IC_{50} μM	RCC4/VHL IC_{50} μM	Ratio[a]
18	Ph	11.6	33.2	2.9	**39**	2-Ph	19.1	40.0	2.1
19	4-pyridyl	13.8	34.0	2.5	**40**	Ph-4-Ac	38.8	33.4	0.9
20	Ph-4-CF_3	12.8	22.6	1.8	**41**	4-pyridyl	28.9	38.0	1.3
21	Ph-4-iPr	>40	>40	ND	**42**	2-pyridyl-6-F	>40	>40	ND
22	Ph-4-$CONH_2$	4.1	1.6	1.6	**43**	5-pyrimidine	26.4	37.0	1.4
23	Ph-4-CONpiperazine-N-methyl	12.8	>40	>3.1	**44**	4-(1*H*-indole)	3.1	4.5	1.5
24	Ph-4-$CONH(CH_2)_3NMe_2$	4.0	3.9	1.0	**45**	3-thiophene	8.7	>40	>4.6
25	Ph-4-SO_2CH_3	1.6	13.4	8.4	**46**	4-(3,5-dimethyloxazole)	3	36.5	12
26	Ph-4-SO_2NHtBu	4.5	22.5	5.0	**47**	3-pyrazole	0.48	20.0	14
27[b]	Ph-4-Ac	3.9	35.1	9	**48**	4-(1-methylpyrazole)	5.2	8.1	1.6
28[b]	$C\equiv CCH_2OH$	0.24	2.9	11.9	**49**	4-(1-benzylpyrazole)	2.2	66.1	30
29[b]	$C\equiv CCH_2OMe$	0.62	27.9	45	**50**	4-(1-benzyltriazole)	2.1	14.0	6.7
30	$C\equiv C(CH_2)_2OH$	1.1	2.8	2.5	**51**	4-methylpiperazine	11.5	31.6	2.8
31	$C\equiv C(CH_2)_3OH$	6.3	0.3	0.1	**52**	$NH(CH_2)_2$Nmorpholine	3.7	8.0	2.2
32	$C\equiv CCH_2$Nmorpholine	0.57	2.3	4.0	**53**	$O(CH_2)_2$Nmorpholine	7.0	21.1	3.0
33	$C\equiv CCH_2$Npiperazine-4-Me	2.6	2.2	0.9	**54**	$O(CH_2)_3NMe_2$	6.0	8.8	1.5
34	4-(1-benzyltriazole)	>40	>40	ND					

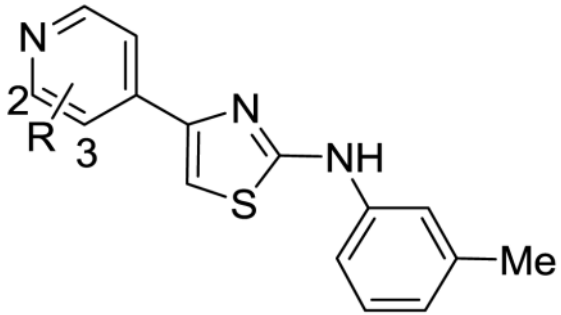

No	3-R	RCC4 IC_{50} μM	RCC4/VHL IC_{50} μM	Ratio[a]	No	2-R	RCC4 IC_{50} μM	RCC4/VHL IC_{50} μM	Ratio[a]
35	4-methylpiperazine	2.6	6.6	2.5					
36	$NH(CH_2)_2$Nmorpholine	19.5	27.9	1.4					
37	$O(CH_2)_2$Nmorpholine	0.32	0.88	2.8					
38	$O(CH_2)_3NMe_2$	2.7	20.2	7.4					

[a] Ratio = IC_{50} (RCC4/VHL)/IC_{50} (RCC4).

[b] Data from reference 20.

Table 4

PAT CoMFA Model.

Model	q^{2a}	SEP[b]	Comp.[c]	r^{2d}	SEE [e]	Steric	Electrostatic
1[5]	0.352	0.431	3	0.818	0.229	0.618	0.382
2	0.270	0.449	4	0.852	0.202	0.549	0.451
3	0.345	0.428	3	0.809	0.231	0.607	0.393
4	0.246	0.475	4	0.831	0.225	0.597	0.403
5	0.423	0.429	5	0.878	0.197	0.552	0.448
6	0.313	0.463	6	0.893	0.182	0.510	0.490

Footnotes: Models 1–6 were constructed as described in the text and the compounds in each set are listed in the Supplementary data.

[a] q^2 is the cross validated r^2 derived from Leave-One-Out SAMPLS (LOO SAMPLS) cross validation analysis as implemented in SYBYL8.2.

[b] SEP is the Standard Error of Prediction reported for the LOO SAMPLS analysis.

[c] Comp. is the number of components used in the model;

[d] r^2, non-cross-validated correlation coefficient.

[e] SEE is the Standard Error of Estimate derived from the Non-Validated analysis.

Table 5

Analysis of the effect of different fragment distinction sets on HQSAR models.

Model	Fragment distinction [a]	q^2 [b]	SE [c]	r^2 [d]	SE [c]	Components	HL [e]
7	None	0.193	0.502	0.408	0.430	6	353
8	A	0.046	0.529	0.256	0.467	6	353
9	A B	0.333	0.442	0.574	0.353	2	353
10	A B C	0.237	0.476	0.572	0.357	3	97
11	A B C H	0.250	0.484	0.705	0.303	6	151
12	A B C D	0.361	0.443	0.793	0.252	5	199
13	A B C H D	0.250	0.484	0.773	0.266	6	199
14	A B H	0.268	0.467	0.522	0.377	3	353
15	A B H D	0.212	0.496	0.794	0.254	6	151
16	A B D	0.082	0.535	0.788	0.257	6	257
17	A C	0.250	0.472	0.588	0.350	3	353
18	A C H	0.281	0.473	0.734	0.288	6	257
19	A C H D	0.201	0.491	0.659	.0321	4	199
20	A C D	0.322	0.456	0.734	0.285	5	97
21	A D	0.028	0.551	0.683	0.314	6	257
22	A H D	0.199	0.488	0.472	0.396	3	199

Footnotes.

[a] Fragment distinction; molecular features to be used in distinguishing among fragments, include A, atom, B, bond, C, connections, H, hydrogens, D, donor acceptor.

[b] q^2, cross validated r^2.

[c] SE, standard error.

[d] r^2, non-cross-validated correlation coefficient. All models were generated using a fragment atom count range of 4 to 7 and selected based on best cross-validated r^2.

[e] HL, Hologram Length.

Table 6

Optimizing fragment size for the HQSAR analysis using fragment distinction (A B C D).

Model	Fragment Size [a]	q^2 [b]	SE [c]	r^2 [d]	SE [c]	Components	HL [e]
23	1-4	0.143	0.505	0.564	0.360	3	353
24	2-5	0.162	0.511	0.768	0.269	6	199
25	3-6	0.226	0.484	0.661	0.329	4	353
26	4-7	0.361	0.443	0.793	0.252	5	199
27	5-8	0.276	0.468	0.732	0.285	4	353
28	6-9	0.334	0.448	0.721	0.290	4	257
29	7-10	0.312	0.463	0.837	0.225	6	257
30	8-11	0.375	0.438	0.782	0.259	5	307
31	9-12	0.331	0.450	0.718	0.292	4	353
32	10-13	0.343	0.449	0.808	0.243	5	257

Footnotes.

[a] Fragment size in atoms.

[b] q^2, cross-validated r^2.

[c] SE, standard error.

[d] r^2, non-cross-validated correlation coefficient. All models were generated using a fragment atom count range of 4 to 7 and selected based on best cross-validated r^2.

[e] HL, Hologram Length.